

# Dynamic contrast-enhanced MR imaging in osteoid osteoma: relationships with clinical and CT characteristics

P. Pottecher<sup>1,2</sup> · E. Sibileau<sup>1</sup> · S. Aho<sup>3</sup> · B. Hamze<sup>1</sup> · C. Parlier<sup>1</sup> · J. D. Laredo<sup>1</sup> · V. Bousson<sup>1</sup>

Received: 14 December 2016 / Revised: 13 March 2017 / Accepted: 27 March 2017 / Published online: 11 April 2017  
© ISS 2017

## Abstract

**Objective** To correlate dynamic contrast-enhanced magnetic resonance imaging (DCE-MRI) features to clinical and computed tomography (CT) morphological features of osteoid osteoma (OO).

**Materials and methods** Our institutional review board approved this retrospective study, waiving the need for informed consent. We included the 102 patients treated with interstitial laser ablation for histologically documented OO at our institution in 2008–2013. DCE-MRI variables were the time-enhancement pattern and rising slope ( $Slope_{rise}$ ) and CT variables were the bone and segment involved ( $OO_{bone}$  and  $OO_{segment}$ , respectively), OO location relative to the native cortex ( $OO_{cortex}$ ), nidus surface area, vessel sign, and largest neighboring-vessel diameter ( $Dmax_{vessel}$ ). Descriptive statistics and correlations linking DCE-MRI findings to clinical and CT characteristics were computed.

**Results** DCE-MRI showed early arterial peak enhancement in 95 (93%) cases, with a mean  $Slope_{rise}$  of  $9.30 \pm 8.10$ . CT

visualized a vessel sign in 84 (82%) cases with a mean  $Dmax_{vessel}$  of  $1.10 \pm 0.60$  mm. By univariate analysis,  $Slope_{rise}$  correlated significantly with pain duration and  $Dmax_{vessel}$  ( $r = 0.30$ ,  $P = 0.003$ ; and  $r = 0.22$ ,  $P = 0.03$ ; respectively). Analysis of variance showed that  $Slope_{rise}$  correlated significantly with  $OO_{bone}$  ( $P < 0.001$ ), with a steeper slope for OOs located in short or flat bones.

**Conclusion** This study suggests more abundant vascularization of OOs with long-lasting pain and location on short or flat bones.

**Keywords** Osteoid osteoma · Dynamic contrast-enhanced MRI · Vessel sign · Vascular groove sign · Pain

## Abbreviations

CT	computed tomography
DCE	dynamic contrast-enhanced
ILA	interstitial laser ablation
MR	magnetic resonance
MRI	magnetic resonance imaging
OO	osteoid osteoma
ROI	region of interest

This work was performed at the Lariboisière Hospital, 2 rue Ambroise Paré, 75475 Paris, FRANCE.

This work has been accepted for an oral presentation at the 2016 European Congress of Radiology meeting.

✉ P. Pottecher  
pierre.pottecher@gmail.com

<sup>1</sup> Department of Osteoarticular Radiology, Hôpital Lariboisière, AP-HP, 2 rue Ambroise Paré, 75475 Paris Cedex 10, France

<sup>2</sup> Department of Vascular, Oncologic and Interventional Radiology, Hôpital du Bocage, 14, rue Paul-Gaffarel, BP 77908, 21079 Dijon cedex, France

<sup>3</sup> Hospital Hygiene and Epidemiology unit, Hôpital du Bocage, BP 77908, 21079 Dijon Cedex, France

## Introduction

Osteoid osteomas (OOs) are benign bone-forming tumors characterized by small size, limited growth potential, and disproportionate pain [1]. They occur chiefly between 7 and 25 years of age [2]. Histology shows a central nidus composed of variably calcified osteoid islands and a capillary network [3]. The nidus has a prominent arterial and arteriolar blood supply [3]. The sclerotic bone surrounding the nidus has also been described as hypervascular [3].

The radiographic and computed tomography (CT) diagnosis of OO is based on visualization of the nidus as a small, round or oval, radiolucency with a variable amount of mineralization, surrounded by reactive sclerotic bone [4]. In most cases, these structural features readily differentiate OO from other lesions such as intracortical or intramedullary abscess, eosinophilic granuloma, herniation pit, intraosseous ganglion cyst, chondroma, chondroblastoma, osteoblastoma, and stress fracture. However, in challenging cases [5], demonstrating a hypervascularity of the nidus can provide crucial diagnostic assistance.

Various imaging techniques have been used to demonstrate the characteristic increase in blood flow within the nidus. In a dynamic magnetic resonance imaging (MRI) study of vascular kinetics, reported in 2003, 9 (82%) of 11 OOs exhibited early peak enhancement at the arterial phase followed by early partial washout [6]. Subsequently, several small studies confirmed that cross-sectional imaging to assess vascular kinetics helped to rule out differential diagnoses and to detect posttreatment recurrences [7–9]. Furthermore, CT often showed a main vessel feeding the nidus (the vessel sign) or grooves extending from the bone surface to the nidus and believed to indicate large feeding arterioles encased in the hyperostotic reaction (vascular groove sign). These findings were highly specific of OO [10, 11]. However, little information is available on potential links between OO vascularization and other characteristics such as natural history of the tumor, age and gender of the patient, bone involved and site of involvement in the bone, and morphologic characteristics of the nidus.

The objective of this study was to correlate DCE-MRI features to clinical and CT morphological features of OO.

## Material and methods

### Study population

Our institutional review board approved the study and waived the need for patient informed consent, in compliance with French law on retrospective studies. From January 2008 to November 2013, 259 patients with clinically and radiologically diagnosed OO underwent interstitial laser ablation (ILA) at our institution. Among them, we included those meeting the following criteria: histological documentation of the diagnosis of OO based on a biopsy taken immediately before ILA, availability of medical records, no previous treatment that might have affected nidus mineralization, and dynamic contrast-enhanced DCE-MRI and CT performed at our institution before ILA and stored in our central database.

Of the 259 patients, 102 met our selection criteria. Reasons for non-inclusion were negative or noncontributive histological findings ( $n = 88$ ), missing clinical data ( $n = 23$ ), MRI

without DCE ( $n = 34$ ), DCE-MRI motion artifacts precluding assessment of enhancement kinetics ( $n = 4$ ), and missing imaging data ( $n = 8$ ). Of the 102 study patients, 69 were also included in another study by our group [12].

There were 63 males and 39 females with a mean age of  $22.6 \pm 10.3$  years (range, 9–50 years; median, 18 years). Mean pain duration was  $16.0 \pm 11.2$  months (range, 3–62 months; median, 12 months). Mean pain duration was  $16.0 \pm 11.2$  months (range, 3–62 months; median, 12 months).

### Clinical parameters

The data were abstracted from reports of the pre-ILA evaluations performed by five musculoskeletal radiologists (35, 18, 24, 20, and 10 years of experience, respectively) and from reports written by senior rheumatologists in the department of patient admission for ILA. The following were collected: gender, age, and pain duration (based on patient-reported month and year of onset and on the date of the first analgesic prescription) [12]. Data were anonymized for the statistical analysis.

### Magnetic resonance imaging (MRI)

#### Image acquisition

A 1.5-T MR system was used (Avanto, Magnetom, Siemens, Erlangen, Germany). T1-weighted turbo spin-echo (SE) (TR = 450–700 ms; TE = 10–12 ms) and T2-weighted fast SE (TR = 3000–4500 ms; TE = 60–80 ms) with fat saturation images were acquired in axial and vertical planes, with a slice thickness of 3 mm. Thereby, the nidus within bone oedema was located.

For the dynamic contrast enhanced study, axial T1-weighted images (TR = 4.52 ms/TE = 1.63 ms) were obtained using a three-dimensional (3D) fast spoiled gradient echo sequence with fat saturation. A bolus of gadoteric acid (Dotarem®, Guerbet, Aulnay, France), 0.15 mmol/kg, was injected into an antecubital vein at about 2 mL/s via an electrically powered infusion pump. DCE-MRI scanning was started simultaneously with the injection and continued for 300 s. Temporal resolution was 30 s from January 2008 to December 2012 (to replicate a previous protocol [6]) and 4 s from January 2013 to November 2013. Flip angle was 30°, matrix 256–256, bandwidth 250, number of excitations 1, acquisition time 30 s, number of sections 10–15, and section thickness 3 to 4 mm. Field of view ranged from 160 to 400 mm.

Seven consecutive dynamic acquisitions with a temporal resolution of 30 s (4 s in 6 cases) were used to establish a time-signal intensity curve.

### Image analysis

Interobserver variability was assessed by having two radiologists (PP and ES, respectively 7 and 10 years of experience with MRI interpretation) calculate  $\text{Slope}_{\text{rise}}$  for 60 randomly selected scans. Both readers were blinded to clinical and morphological CT data.

DCE-MRI data were analyzed on a commercially available workstation using dedicated software (Multi Workstation MMWP, DynamicMRI application, Siemens, Erlangen, Germany). Time-signal intensity curves for the entire dynamic MRI acquisition (300 s) were plotted within regions of interest (ROI) in the nidus, an artery, the adjacent bone marrow (free of edema), and muscle. The nidus was identified on the conventional sequences and seven consecutive dynamic acquisitions. Then, an ovoid ROI including as much of the enhanced nidus as possible but excluding the surrounding rim of sclerosis was drawn (Fig. 1). The curve of the arterial blood vessel served as a control for adequate injection technique and as a reference for a typical pattern of arterial enhancement [13].

**Qualitative DCE-MRI parameters** For qualitative analyses, curve morphology was analyzed according to the classification developed by van Rijswijk et al. [14]: type I, flat curve; type II, progressive enhancement with no enhancement peak; type III, enhancement peak followed by a plateau; type IV, enhancement peak followed by washout; and type V, enhancement peak followed by progressive enhancement.

**Semi-quantitative DCE-MRI parameters** Rising slope ( $\text{Slope}_{\text{rise}}$ ) was computed based on a time-signal intensity (SI) curve (Fig. 1). Baseline SI ( $\text{SI}_{\text{base}}$ ) was defined as the mean SI on the non-contrast-enhanced T1-weighted images and maximum SI ( $\text{SI}_{\text{max}}$ ) as the maximum value of the ascending limb of the curve [15, 16]. The contrast enhancement rise time,  $T_{\text{rise}}$ , was defined as the time from  $\text{SI}_{\text{base}}$  to  $\text{SI}_{\text{max}}$ .  $\text{Slope}_{\text{rise}}$  was computed for each ROI as  $(\text{SI}_{\text{max}} - \text{SI}_{\text{base}}) / T_{\text{rise}}$ .

### CT imaging

#### Image acquisition

CT was performed before ILA procedure, to select the percutaneous approach. A 64-row CT scanner (Sensation 64, Somatom, Siemens, Erlangen, Germany) was used, with the following acquisition parameters: 120 kV, rotation time 1 s, section collimation 0.6 mm, pitch factor 0.90, matrix 512·512, field of view 8–10 cm as appropriate for each location, and 120–150 mA. CT images were reconstructed with 1-mm section thickness, 1.0-mm interval, and a medium sharp reconstruction algorithm (B50 kernel).

### Image analysis

CT data were obtained from bone-window images (window width, 3500 HU; window center, 400 HU) with multiplanar reconstruction on a Vue PACS workstation (version 11.3, Carestream Health, Rochester, NY).

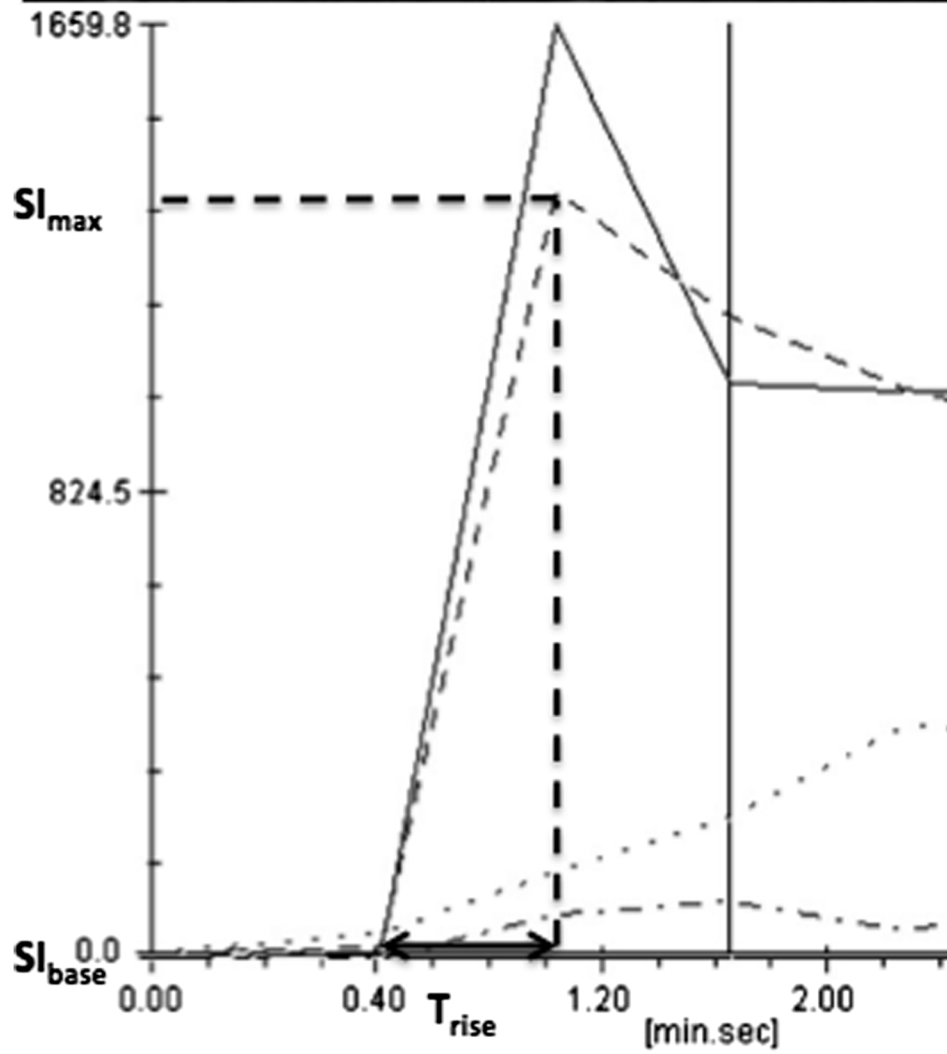
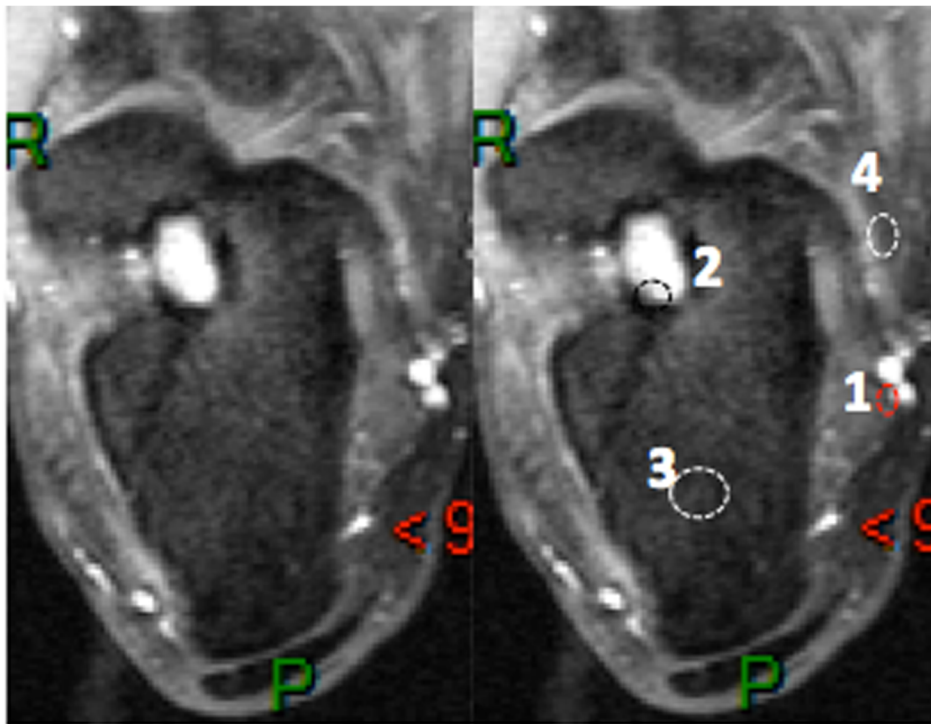
The following morphological variables were assessed for each OO: (a) The bone involved ( $\text{OO}_{\text{bone}}$ ); (b) for long bones, the segment involved, i.e., the diaphysis, metaphysis, or epiphysis ( $\text{OO}_{\text{segment}}$ ); (c) the location of the nidus center relative to the native cortex ( $\text{OO}_{\text{cortex}}$ ), which was used to classify OOs as subperiosteal, intracortical, endosteal, or within the cancellous bone; (d) intra- or extraarticular location ( $\text{OO}_{\text{articular}}$ ); and (e) nidus surface area ( $\text{mm}^2$ ) in two perpendicular planes, after using the mouse to delineate the nidus contours on bone-window CT images. The largest surface area ( $\text{Nidus}_{\text{area}}$ ) was recorded (Fig. 2).

#### Vessel sign or vascular groove sign

One radiologist (PP, 7 years of experience interpreting CT images and 2 years of specialization in musculoskeletal imaging) evaluated the blood vessels visible near the OO on CT images. A blood vessel was defined as a radiolucent linear or serpiginous groove extending from the cortex and periosteal surface of the bone down to, or close to, the radiolucent nidus (Fig. 3a). For each OO, the following were recorded: (a) presence or absence of a blood vessel on multiplanar reconstructions; (b) number of blood vessels ( $N_{\text{vessel}}$ ); and (c) diameter of each vessel ( $D_{\text{vessel}}$ , mm) measured using Image J software (<http://rsb.info.nih.gov/ij/>) [17]. CT images were registered in DICOM format. Figure 3b illustrates the steps performed to measure  $D_{\text{vessel}}$ . First, the bone window was inverted to better identify the cortical bone delimiting the vessel. Then, a line was traced perpendicularly to the main axis of the vessel selected to create the gray value profile. The profile was associated with a coordinate system. The borders of the groove were identified based on a dramatic change in the pixel gray value along the profile. The vessel diameter was obtained from the coordinates. For serpiginous vessels,  $D_{\text{vessel}}$  was measured at the periosteal surface. When several vessels were visible,  $D_{\text{vessel}}$  was determined for each. The largest diameter for each OO ( $D_{\text{max,vessel}}$ , in mm) was recorded and used for the statistical analysis (Fig. 3c).

Interobserver variability was evaluated by having a second radiologist (ES, with 15 years of experience interpreting CT images and 5 years of specialization in musculoskeletal imaging) record these three variables on 30 randomly selected CT scans, 2 months after the first reader (PP).

Figure 4 recapitulates the variables determined by DCE-MRI and CT.



◀ **Fig. 1** Semi-quantitative DCE-MRI parameters: osteoid osteoma of the calcaneus in a 12-year-old boy. The four regions of interest contain an artery (1), the tumor (2), non-edematous adjacent bone (3), and soft tissue (4), respectively. Time-intensity curve with rising slope ( $Slope_{rise}$ ) computed as  $(SI_{max} - SI_{base}) / T_{rise}$ .  $Slope_{rise}$ , rising slope;  $SI_{max}$ , maximal signal intensity;  $SI_{base}$ , signal intensity at baseline;  $T_{rise}$ , contrast enhancement rise time; ART, arterial fraction; OO, osteoid osteoma

### Statistical analysis

To assess agreement for quantitative variables ( $Slope_{rise}$ ,  $D_{max_{vessel}}$ ), we computed Lin's concordance correlation coefficient ( $\rho_c$ ) [18]. The kappa coefficient ( $\kappa$ ) was computed to evaluate agreement for  $N_{vessel}$ . Each quantitative variable was described as the mean, standard deviation, median, and range of values.

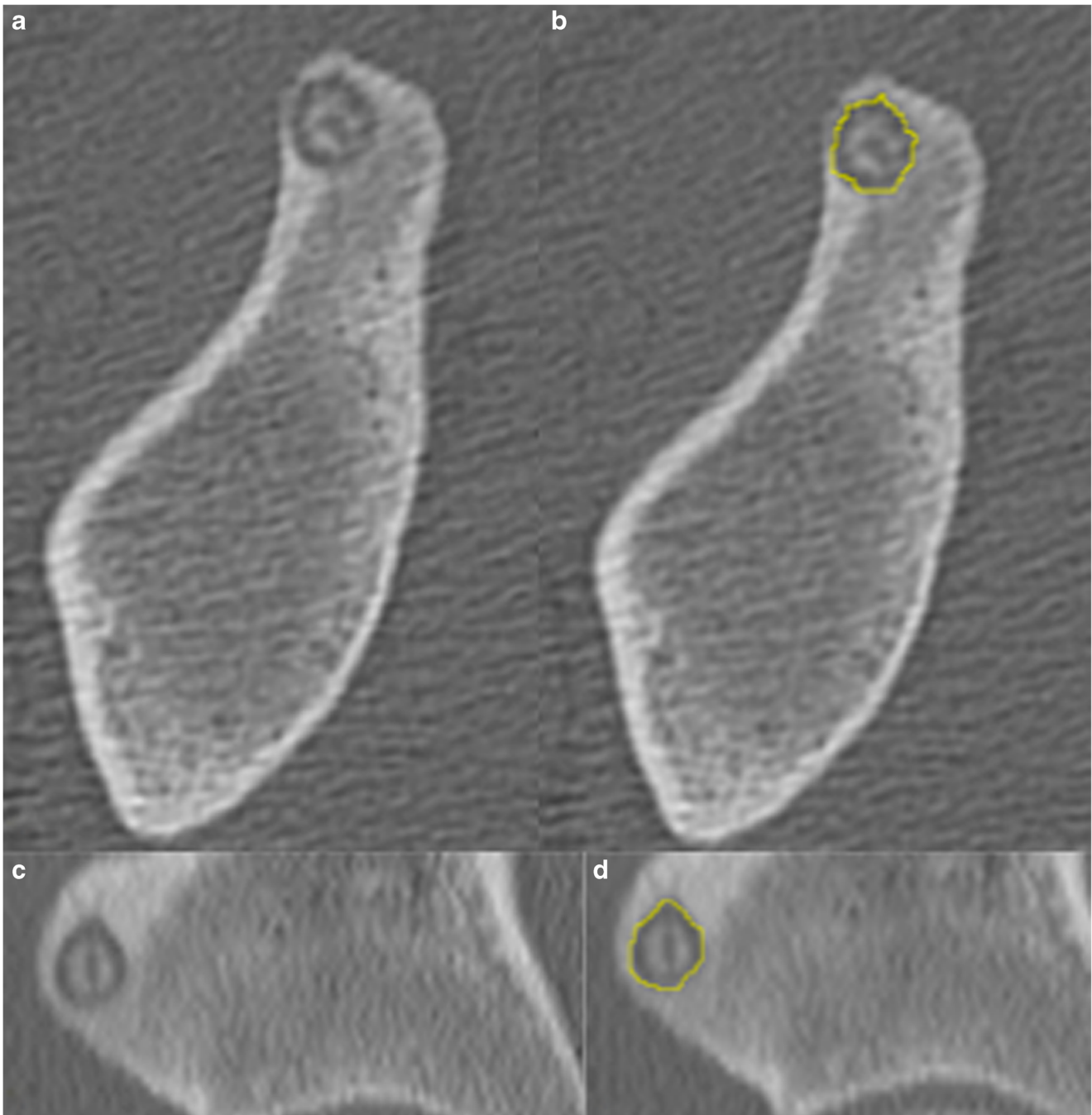


**Fig. 2** Determination of the surface area of the nidus ( $Nidus_{area}$ ): osteoid osteoma of the acetabulum in a 9-year-old girl (**a, c**) Transverse CT images and (**b, d**) sagittal reformations. The nidus contours were delineated in both planes (**c, d**), and the greatest of the two values was recorded

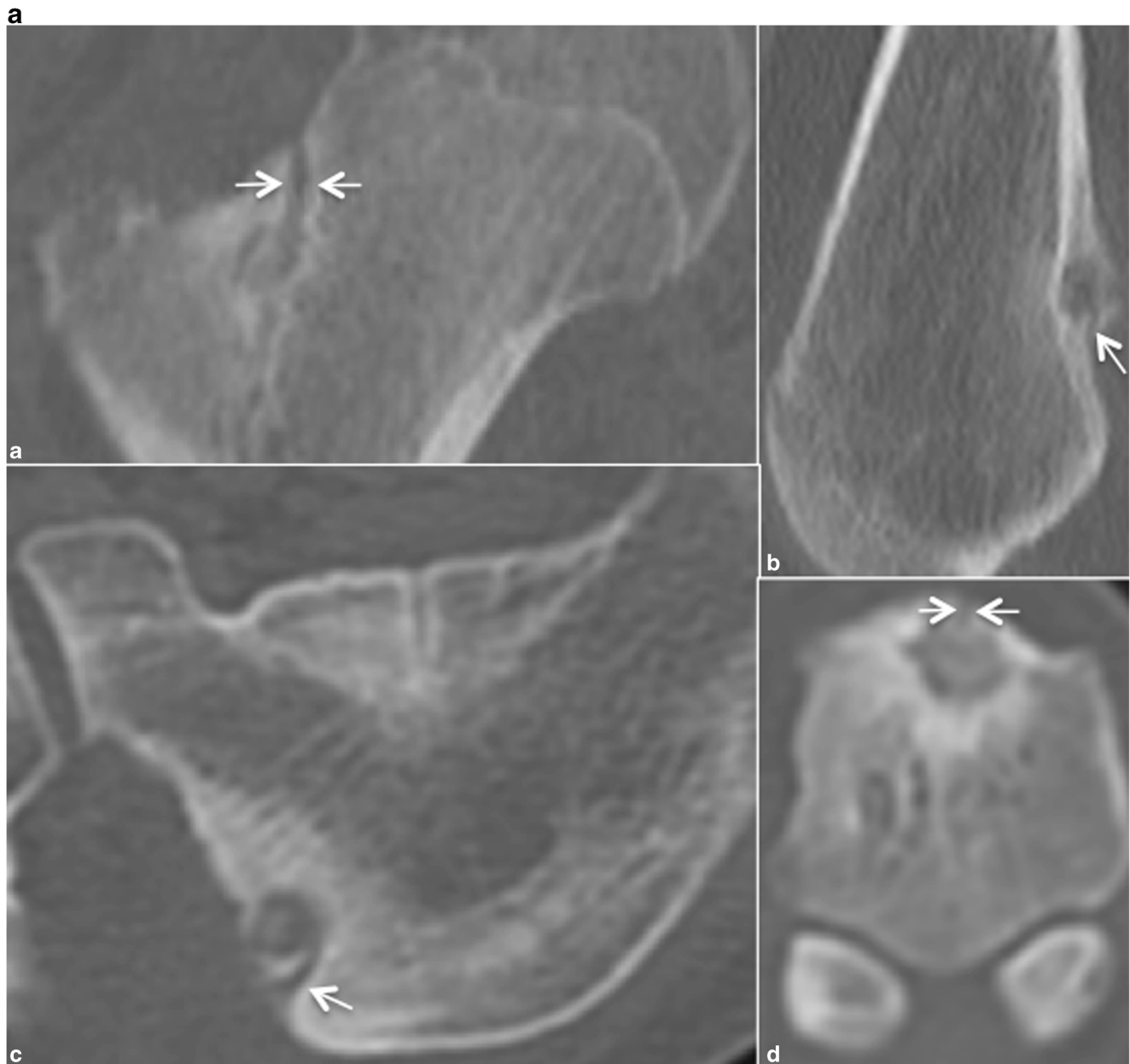


**Fig. 3** **3a** Computed tomography appearance of a vessel feeding the nidus: Four The CT data were analyzed on bone-windowed images (window width, 3500 HU; window center level, 400 HU) and multiplanar reconstructions. A blood vessel (*arrow*) was seen as a radiolucent linear or serpiginous groove extending from the cortex and periosteal surface of the bone down to the radiolucent nidus. **(a)** 15-year-old boy: osteoid osteoma of the femoral metaphysis with a large feeding vessel **(b)** 34-year-old male: subperiosteal osteoid osteoma of the femoral diaphysis **(c)** 12-year-old boy: osteoid osteoma of the calcaneus with a single feeding vessel **(d)** 38-year-old female: osteoid osteoma of the first metatarsal bone. **3b** Steps used to measure vessel diameter with ImageJ

Subperiosteal OO of the femoral diaphysis in a 12-year-old girl CT images are registered in DICOM format **(a)**. The bone window is inverted to better identify the bone delimiting the vessel **(b)**; a line is drawn perpendicularly to the main axis of the vessel (in yellow). Gray level intensity (coordinate Y) and the corresponding coordinate along this line (X) are used to determine the diameter of the vessel **(c)**. In this example, vessel diameter was 1.25 mm. **3c** Determination of the largest vessel diameter ( $D_{\max_{\text{vessel}}}$ ) Subperiosteal OO of the femoral diaphysis in a 9-year-old boy Three vessels feeding the nidus are visible. Their diameters ( $D_{\text{vessel}}$ ) are 1.01 mm, 1.01 mm, and 0.76 mm, respectively. Therefore,  $D_{\max_{\text{vessel}}} = 1.01$  mm

To look for relationships linking DCE-MRI parameters to clinical and morphological CT features, we first performed univariate analyses of all variables. Those variables associated with  $P$  values  $<0.1$  were then entered into a multivariate linear regression model with a robust variance estimator, using a

manual backward procedure. Fractional polynomials were computed to check linearity [19]. Relationships between clinical and CT parameters were assessed using linear regression (including categorical predictors) with a robust variance estimator.

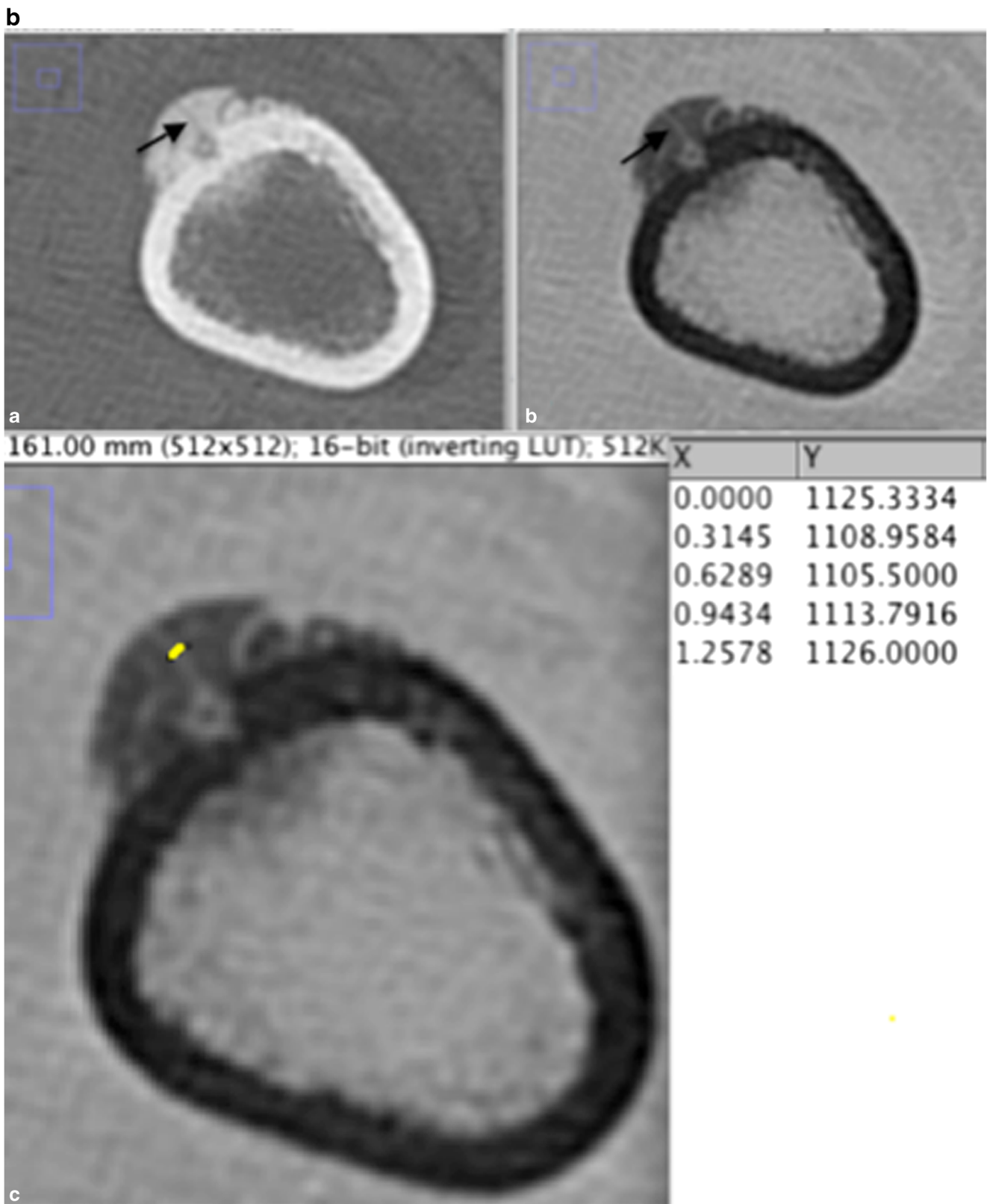


**Fig. 3** (continued)

Confidence intervals (CIs) were set at 95%. All statistical analyses were performed using Stata software, version 12.0

(Stata, College Station, TX). *P* values less than 0.05 were considered significant.

**c**

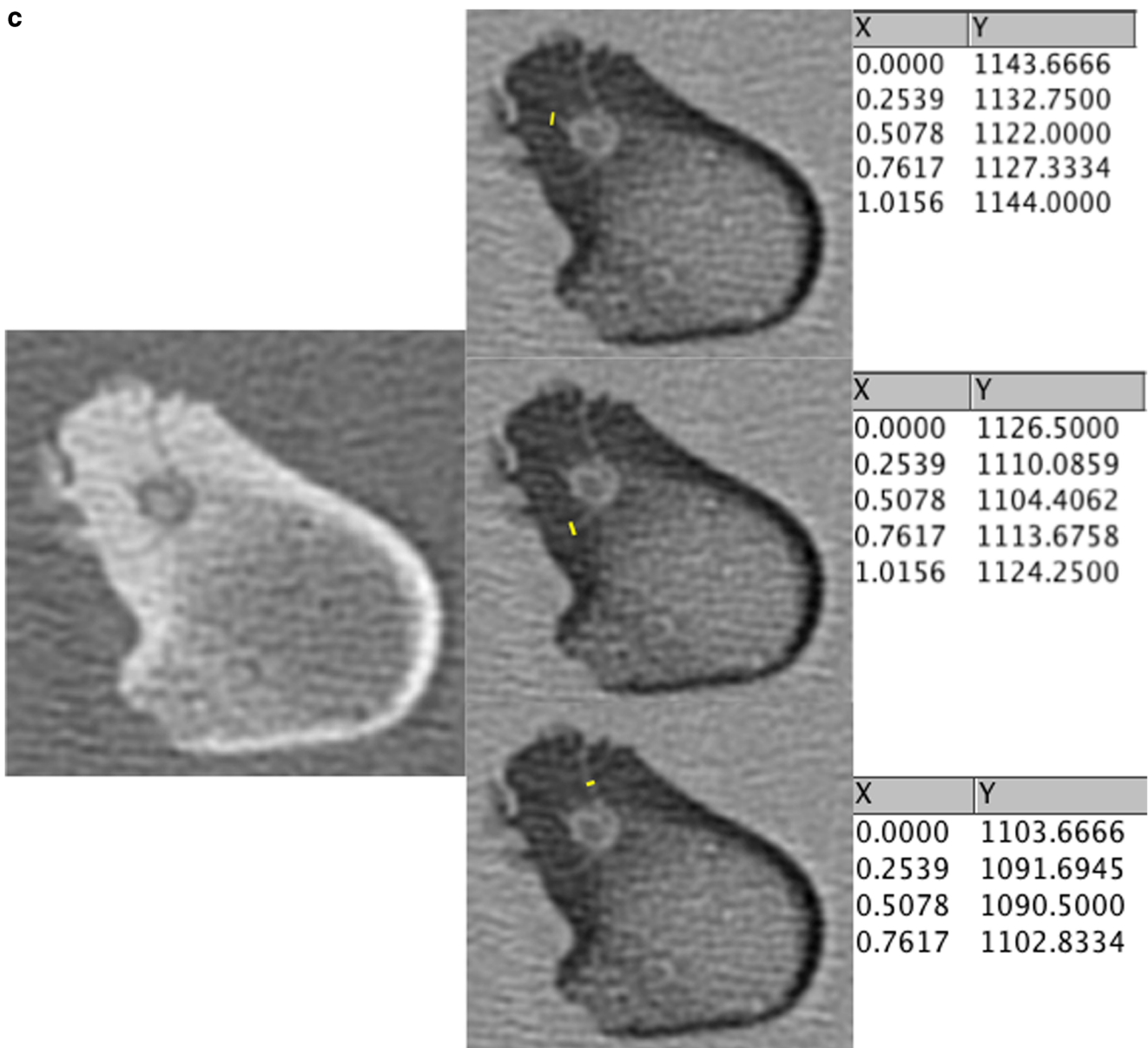


Fig. 3 (continued)

**Results**

**Interobserver agreement**

Interobserver agreement between the two radiologists for Slope<sub>rise</sub> measurement was very good ( $\rho_c = 0.987$ ,  $P < 0.001$ ).

Regarding CT parameters, interobserver agreement was perfect for identification of a vessel to the nidus, with the lower boundary of the 95% CI at 87%; substantial for  $N_{vessel}$  ( $\kappa = 0.78$ ; 95% CI, 0.39–1.17); and very good for  $Dmax_{vessel}$  ( $\rho_c = 0.857$ ,  $P < 0.001$ ).

For the statistical analysis, only  $Dmax_{vessel}$  was tested.

**Fig. 4** CT and DCE-MRI images in 2 patients. **4a** 13-year-old boy: intracortical OO of the femoral metaphysis with a vessel feeding the nidus (arrow) (a). Corresponding axial T1-weighted sequence (b) and T2-weighted sequence with fat saturation (c) showing marked edema of the bone and surrounding soft tissue. Enhancement kinetics curve (d): early enhancement peak followed by washout (Type IV according to van Rijswijk et al.). **4b** 37-year-old male: subperiosteal OO of the femoral metaphysis with no visible feeding vessel (a). Corresponding axial T1-weighted sequence (b) and T2-weighted sequence with fat saturation (c) showing moderate bone edema. Axial T1-weighted images with dynamic contrast enhancement (d) at the arterial/venous phase (75') with the corresponding enhancement kinetics curve (e): gradual enhancement with a delayed peak (type II according to van Rijswijk et al.) Art. arterial fraction; OO, osteoid osteoma y axis represents signal intensity (SI) measurements



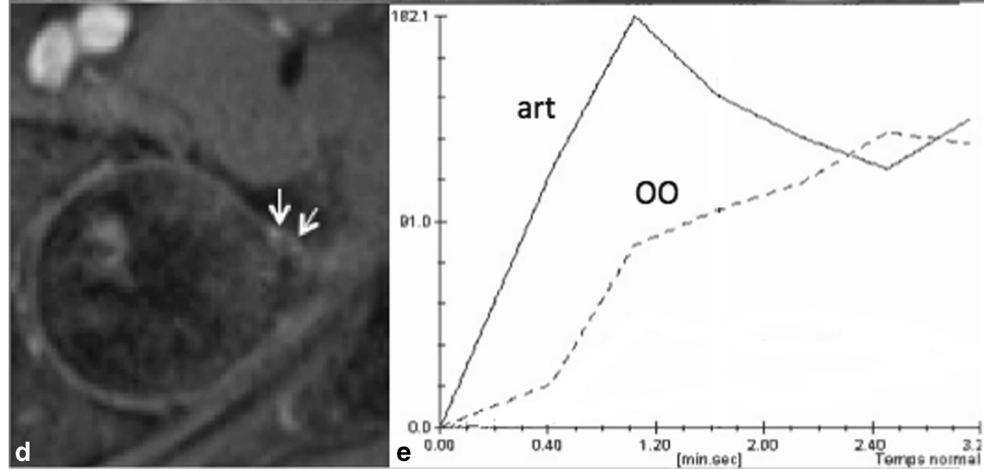
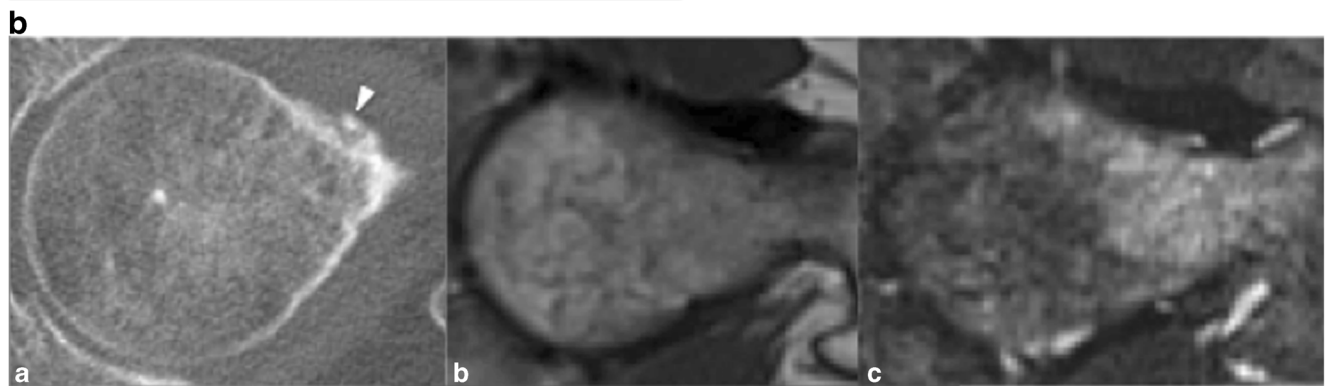
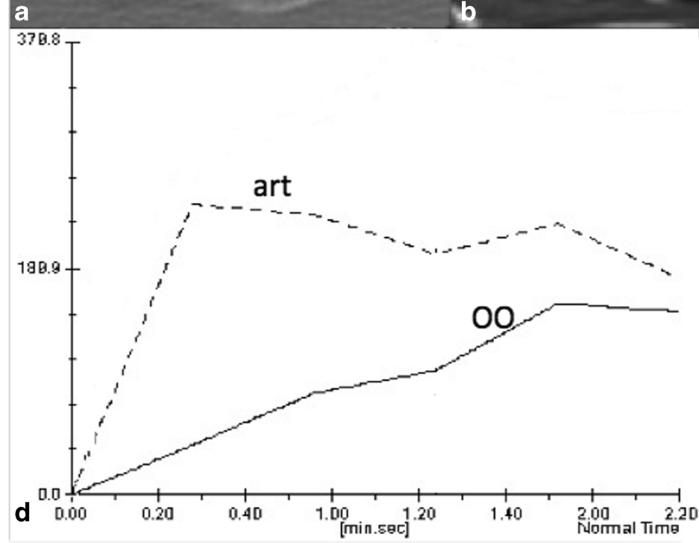
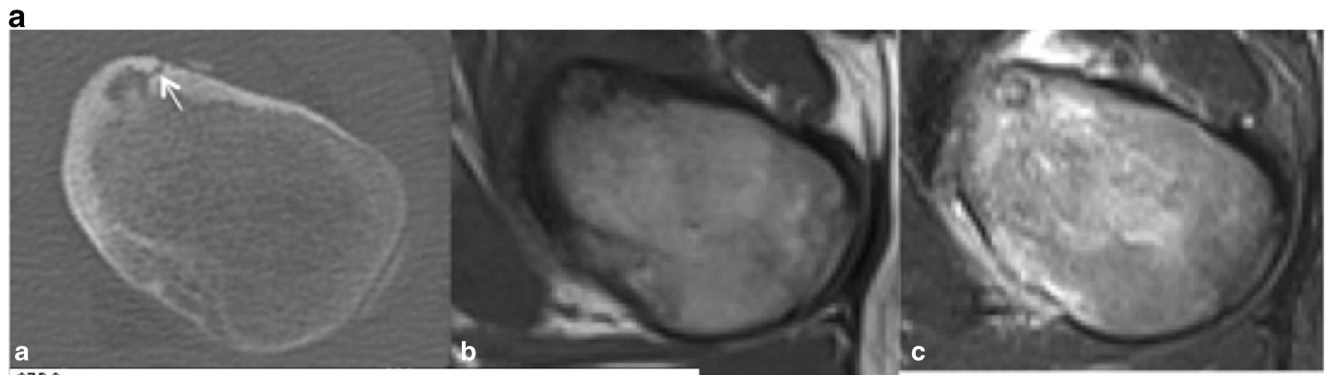


**Table 1** Location of the 102 osteoid osteomas

Location	N. of patients
Bone	102
Femur	51
Fibula	2
Tibia	21
Humerus	4
Ulna	1
Radius	1
Calcaneus	3
Metatarsus	1
Patella	1
Talus	1
Acetabulum	9
Ilium	3
Vertebrae	4

## Descriptive analysis

### DCE-MRI parameters

Enhancement kinetics were type IV in 62 (61%) patients, type III in 33 (32%), and type II in 7 (7%). Thus, an early arterial

peak was observed in 95 (93%) patients. Overall mean  $Slope_{rise}$  was  $9.3 \pm 8.1$  (range, 0.46–48.92; median, 7.10).

### CT parameters (Table 1)

OO locations are reported in Table 1 and Fig. 5. Most OOs were extraarticular (82/102, 80.4%). Mean  $Nidus_{area}$  was  $40.10 \pm 28.84 \text{ mm}^2$  (range, 7.5–174.66  $\text{mm}^2$ ; median, 34.30  $\text{mm}^2$ ). A vessel was visible in 84 (82.3%) patients; of the 18 OOs with no visible vessel, 14 were in long bones and 4 in flat bones (acetabulum and vertebrae, 2 cases each). Mean  $D_{max_{vessel}}$  was  $1.10 \pm 0.66 \text{ mm}$  (range, 0.4–3.8 mm; median, 1.20 mm).

### Univariate analysis

*Relationships linking  $Slope_{rise}$  to clinical and CT features (Table 2)*

$Slope_{rise}$  was neither significantly related to age ( $r = 0.16$ ,  $P = 0.116$ ) nor significantly different between males and females ( $P = 0.380$ ).  $Slope_{rise}$  showed a significant positive correlation with pain duration.  $Slope_{rise}$  differed significantly between OOs on long vs. flat/short bones ( $OO_{bone}$ ) but not with

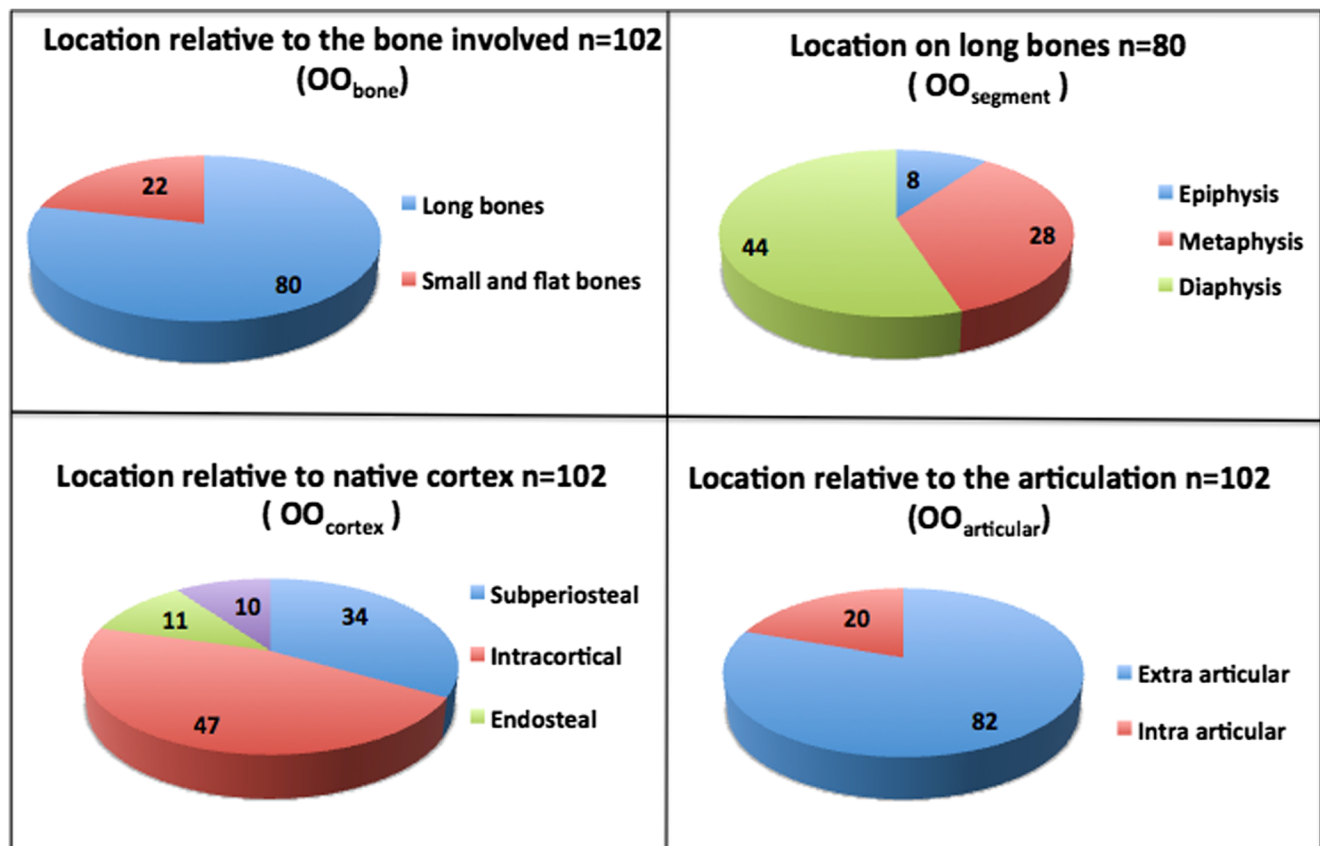


**Fig. 5** Pie charts of the location of the 102 osteoid osteomas (OOs) regarding type of bone ( $OO_{bone}$ ), segment involved on long bones ( $OO_{segment}$ ), position relative to the native cortex ( $OO_{cortex}$ ), and position relative to the nearest articulation ( $OO_{articular}$ )

**Table 2** Relation of Slope<sub>rise</sub> with clinical and CT parameters

		Slope <sub>rise</sub>			
		Linear regression		Analysis of variance	
		<i>r</i>	<i>p</i> value	mean (SD)	<i>p</i> value
Clinical parameters	Genre				0.380
	Male	–		9.9 (9.6)	
	Female			8.4 (4.8)	
	Age	0.16	0.116	–	
	PainD	0.30	0.003	–	
CT parameters	OO <sub>location</sub>	–			0.003
	Long bones			8 (5.2)	
	Flat/ Small bones			13.7 (13.6)	
	OO <sub>segment</sub>	–			0.646
	diaphysis			8.1 (5.1)	
	epiphysis			6.4 (3.7)	
	metaphysis			8.1 (5)	
	OO <sub>cortex</sub>	–			0.056
	intra-cortical			7.8 (5.2)	
	medullary canal -endosteal			15 (16.1)	
	sub-periosteal			9.1 (6.2)	
	OO <sub>articular</sub>	–			0.416
	intra-articular			7.1 (5.5)	
	extra-articular			9.5 (6.45)	
	OO <sub>vessel</sub>	–			0.149
	Present			9.9 (8.7)	
Absent			6.7 (3.2)		
	Dmax <sub>vessel</sub>	0.22	0.031		
	Nidus <sub>area</sub>	0.15	0.149		

Slope<sub>rise</sub>: The slope of the DCE-MRI time intensity curve during enhancement of the osteoid osteoma

Dmax<sub>vessel</sub> in mm; Nidus<sub>area</sub> in mm<sup>2</sup>; Pain<sub>D</sub> in months

*r* Pearson correlation coefficient

the segment involved on long bones (OO<sub>segment</sub>), location relative to the native cortex (OO<sub>cortex</sub>), or intraarticular/extraarticular location (OO<sub>articular</sub>).

Slope<sub>rise</sub>, although not significantly related to Nidus<sub>area</sub>, showed a significant positive correlation with Dmax<sub>vessel</sub>.

#### Relationships linking clinical to CT features (Table 3)

Age showed a significant negative correlation with Dmax<sub>vessel</sub>. Pain duration did not correlate significantly with Dmax<sub>vessel</sub> but showed a significant positive correlation with Nidus<sub>area</sub>. Pain duration was significantly longer in short or flat bone OOs than in long bone OOs. Nidus<sub>area</sub> was significantly larger for metaphyseal than for epiphyseal or diaphyseal OOs. Dmax<sub>vessel</sub> increased with Nidus<sub>area</sub>.

## Discussion

We described the DCE-MRI parameters and assessed their associations with clinical and morphological CT features in 102 patients with histologically proven OO. We found clear evidence of arterial and arteriolar blood supply to the OO nidus, with arterial enhancement in all but 7 cases. These 7 OOs, six with 30 s and one with 6 s DCE-MRI temporal resolution, exhibited gradual enhancement with no arterial peak.

Earlier studies, which had smaller sample sizes, found similarly high prevalences of arterial enhancement (82% [6], 89.5% [7], and 100% [20]). Thus, arterial enhancement strongly suggests a diagnosis of OO when doubt exists regarding osteomyelitis (Brodie's abscess), which produces slow enhancement with no arterial peak [21]. Arterial enhancement may also help to diagnose recurrent OO after percutaneous

**Table 3** Relation between clinical and CT parameters

	Dmaxvessel				PainD				Nidusarea			
	Linear regression		Analysis of variance		Linear regression		Analysis of variance		Linear regression		Analysis of variance	
	<i>r</i>	<i>p</i> value	mean (SD)	<i>p</i> value	<i>r</i>	<i>p</i> value	mean (SD)	<i>p</i> value	<i>r</i>	<i>p</i> value	mean (SD)	<i>p</i> value
Clinical parameters												
Age	0.27	0.005	–	–	0.03	0.778	–	–	0.02	0.872	–	–
PainD	0.08	0.422	–	–	–	–	–	–	0.20	0.049	–	–
OOlocation					–	–			–	–		0.238
Long bones			1.12 (0.68)				14.77 (10.05)				38.37 (13.40)	
Flat/ Small bones			1.04 (5.60)	0.631			20.14 (14.05)	0.048			46.79 (21.40)	
OOsegment					–	–			–	–		<0.001
diaphysis			1.13 (0.55)				14.10 (11.04)				28.75 (9.10)	
epiphysis			0.76 (0.60)				13.42 (6.34)				30.15 (12.61)	
metaphysis			1.19 (0.85)				14.56 (8.20)				56.75 (25.32)	
CT parameters					0.08	0.422			0.26	0.009		
Dmaxvessel			–				–				–	

Dmax<sub>vessel</sub> in mm; Nidus<sub>area</sub> in mm<sup>2</sup>; PainD in months

*r* Pearson correlation coefficient

treatment [20], as it contrasts with the delayed gradual enhancement or absence of enhancement seen in successfully treated patients.

The rate of contrast uptake by the nidus (Slope<sub>rise</sub>) was independent from age and gender but increased significantly with pain duration. To our knowledge, this finding has not been reported previously. It suggests gradual development over time of the arterial blood supply to the nidus of painful OOs. In our experience, many patients report initial moderate pain with mechanical characteristics followed by progression to severe intense inflammatory pain. This time course suggests that expansion of the arterial blood supply may be associated with the development of a nerve supply [3] and with increasing prostaglandin release [22] in the nidus, resulting in increasingly severe and inflammatory pain. Importantly, OOs can be painless or resolve spontaneously with resolution of the initial pain [23]. However, only patients with pain were included in our study.

A new finding from our study is the faster contrast uptake by the nidus in flat and short bones than in long bones. Anecdotal case-reports have established that OOs in flat or short bones receive an arterial blood supply (wrist [24], hand and vertebrae [25], and scaphoid [26]). The more abundant vascularization of OOs in flat and short bones is consistent with the longer pain duration in this tumor-location group. The contrast uptake rate by the nidus tended to be higher in medullary and endosteal OOs than in intracortical and subperiosteal OOs. Conceivably, the vessels from the marrow and endosteum may penetrate the nidus more easily compared to vessels from the periosteum. Also, the more vigorous bone formation in intracortical and subperiosteal OOs compared to medullary and endosteal OOs may create an obstacle to the penetration of vessels into the nidus.

Most of our patients had one or more visible vessels feeding the nidus, in keeping with earlier data from smaller studies (79.6% [10] and 75% [11]). The contrast uptake rate increased significantly with the diameter of the largest feeding vessel, suggesting that this vessel carried arterial blood, in agreement with previous angiographic [24, 25] and histologic [3] data. That nidus surface area increased significantly with the diameter of the largest feeding vessel also supports an active role of this vessel in providing arterial blood. Hypotheses regarding the pathogenesis of OO include neoplasia [27], a possibility challenged by the limited growth potential of these tumors [28]; inflammation [23]; and vascular malformation [29, 30]. OOs share several features with intracortical hemangioma [31] and have been reported in association with the vascular malformation blue rubber-bleb nevus syndrome [32].

Limitations of our study include the low temporal resolution of only 30 s of DCE-MRI in most patients (*n* = 96), which may have been suboptimal for determining Slope<sub>rise</sub>. This

resolution was chosen to allow comparisons with data from an earlier study [6]. The Nyquist limit was markedly lower with the temporal resolution of 4 s used during the last study year than with the 30s resolution used previously. To eliminate the Nyquist limit, a temporal resolution of 3 s would be required. Second, vessel number and diameter are challenging to measure by CT, given the limited spatial resolution of the images compared to actual vessel size. Therefore, vessel diameter may have been overestimated in our study. Third, enhancement by DCE-MRI varies with several parameters [33] such as microvessel density, perfusion rate, permeability, and pressures within the nidus. However, we focused on qualitative and semi-quantitative parameters, without computing quantitative parameters.

## Conclusion

The early arterial peak enhancement in 93% of cases and significant positive correlation between the rate of contrast uptake by DCE-MRI and the diameter of the nidus feeding vessel by CT indicate that the OO nidus receives arterial blood. We found that this supply was more prominent in patients with a long history of pain and in those with involvement of a flat or short bone.

## Compliance with ethical standards

**Disclosure of interest** The authors have no conflict of interest to declare.

## References

- World Health Organization of Tumours. Osteogenic tumours. In: Pathology and Genetics of tumours of soft tissue and bone. IARC; 2013. p. 260–3.
- Resnick DR, Greenway G. Tumors and tumor-like lesions of bone: imaging and pathology of specific lesions. In: Resnick DR, editor. Bone and joint imaging. Philadelphia: Saunders; 1996. p. 1120–30.
- De Chadarevian J-P, Katsetos CD, Pascasio JM, Geller E, Herman MJ. Histological study of osteoid osteoma's blood supply. *Pediatr Dev Pathol*. 2007;10(5):358–68.
- Chai JW, Hong SH, Choi J-Y, et al. Radiologic diagnosis of osteoid osteoma: from simple to challenging findings. *Radiographics*. 2010;30(3):737–49.
- Bece F, Theumann N, Rochette A, et al. Osteoid osteoma and osteoid osteoma-mimicking lesions: biopsy findings, distinctive MDCT features and treatment by radiofrequency ablation. *Eur Radiol*. 2010;20(10):2439–46.
- Liu PT, Chivers FS, Roberts CC, Schultz CJ, Beauchamp CP. Imaging of osteoid osteoma with dynamic gadolinium-enhanced MR imaging. *Radiology*. 2003;227(3):691–700.
- Zampa V, Bargellini I, Ortori S, Faggioni L, Cioni R, Bartolozzi C. Osteoid osteoma in atypical locations: the added value of dynamic gadolinium-enhanced MR imaging. *Eur J Radiol*. 2009;71(3):527–35.
- Von Kalle T, Langendorfer M, Fernandez FF, Winkler P. Combined dynamic contrast-enhancement and serial 3D-subtraction analysis in magnetic resonance imaging of osteoid osteomas. *Eur Radiol*. 2009;19(10):2508–17.
- Gondim Teixeira PA, Lecocq S, Louis M, et al. Wide area detector CT perfusion: can it differentiate osteoid osteomas from other lytic bone lesions? *Diagn Interv Imaging*. 2014;95(6):587–94.
- Yaniv G, Shabshin N, Sharon M, et al. Osteoid osteoma - the CT vessel sign. *Skelet Radiol*. 2011;40(10):1311–4.
- Liu PT, Kujak JL, Roberts CC, de Chadarevian J-P. The vascular groove sign: a new CT finding associated with osteoid osteomas. *AJR Am J Roentgenol*. 2011;196(1):168–73.
- Touraine S, Emerich L, Bissere D, et al. Is pain duration associated with morphologic changes of osteoid osteomas at CT? *Radiology*. 2014;271(3):795–804.
- Van der Woude HJ, Verstraete KL, Hogendoorn PC, Taminiau AH, Hermans J, Bloem JL. Musculoskeletal tumors: does fast dynamic contrast-enhanced subtraction MR imaging contribute to the characterization? *Radiology*. 1998;208(3):821–8.
- Van Rijswijk CS, Geirnaert MJ, Hogendoorn PC, et al. Soft-tissue tumors: value of static and dynamic gadopentetate dimeglumine-enhanced MR imaging in prediction of malignancy. *Radiology*. 2004;233(2):493–502.
- Chen L, Ding X-Y, Wang C-S, Si M-J, Du L-J, Lu Y. Triple-phase dynamic MRI: a new clue to predict malignant transformation of giant cell tumor of bone. *Eur J Radiol*. 2014;83(2):354–9.
- Chen BB, Hsu CY, Yu CW, et al. Dynamic contrast-enhanced MR imaging measurement of vertebral bone marrow perfusion may be indicator of outcome of acute myeloid leukemia patients in remission. *Radiology*. 2011;258(3):821–31.
- Barboriak DP, Padua AO, York GE, Macfall JR. Creation of DICOM-aware applications using ImageJ. *J Digit Imaging*. 2005;18(2):91–9.
- Lin LI. A concordance correlation coefficient to evaluate reproducibility. *Biometrics*. 1989;45(1):255–68.
- Royston P, Ambler G, Sauerbrei W. The use of fractional polynomials to model continuous risk variables in epidemiology. *Int J Epidemiol*. 1999;28(5):964–74.
- Teixeira PAG, Chanson A, Beaumont M, et al. Dynamic MR imaging of osteoid osteomas: correlation of semiquantitative and quantitative perfusion parameters with patient symptoms and treatment outcome. *Eur Radiol*. 2013;23(9):2602–11.
- Woertler K. Benign bone tumors and tumor-like lesions: value of cross-sectional imaging. *Eur Radiol*. 2003;13(8):1820–35.
- Greco F, Tamburrelli F, Ciabattini G. Prostaglandins in osteoid osteoma. *Int Orthop*. 1991;15(1):35–7.
- Goto T, Shinoda Y, Okuma T, et al. Administration of nonsteroidal anti-inflammatory drugs accelerates spontaneous healing of osteoid osteoma. *Arch Orthop Trauma Surg*. 2011;131(5):619–25.
- O'Hara 3rd JP, Tegtmeier C, Sweet DE, McCue FC. Angiography in the diagnosis of osteoid-osteoma of the hand. *J Bone Joint Surg Am*. 1975;57(2):163–6.
- Crouzet G, Mnif J, Vasdev A, Pascal-Ortiz D, Chirossel JP, Pasquier B. Osteoid osteoma of the spine: radiological aspects and value of arteriography. Four cases *J Neuroradiol*. 1989;16(2):145–59.
- Kussman SR, Thompson M, Chang EY. Osteoid osteoma of the scaphoid: magnetic resonance imaging vessel sign. *Clin Imaging*. 2015;39(4):725–7.
- Jaffe HL. "osteoid-osteoma"—a benign osteoblastic tumour composed of osteoid and atypical bone. *Arch Surg*. 1935;31:709–28.
- Gilday DL, Ash JM. Benign bone tumors. *Semin Nucl Med*. 1976;6(1):33–46.
- Rosenthal DI, Hornicek FJ, Wolfe MW, Jennings LC, Gebhardt MC, Mankin HJ. Percutaneous radiofrequency coagulation of

- osteoid osteoma compared with operative treatment. *J Bone Joint Surg Am.* 1998;80(6):815–21.
30. Mullin DM, Rodan BA, Bean WJ, Sehayik S, Sehayik R. Osteoid osteoma in unusual locations: detection and diagnosis. *South Med J.* 1986;79(10):1299–301.
  31. Schajowicz F, Rebecchini AC, Bosch-Mayol G. Intracortical haemangioma simulating osteoid osteoma. *J Bone Joint Surg Br.* 1979;61(1):94–5.
  32. Palleschi GM, Torchia D, Fabbri P. Blue rubber-bleb nevus syndrome: report of a case associated with osteoid osteomas. *J Dermatol.* 2005;32(7):589–93.
  33. Cuenod CA, Balvay D. Perfusion and vascular permeability: basic concepts and measurement in DCE-CT and. *Diagn Interv Imaging.* 2013;94(12):1187–204.